THE JOURNAL OF PHYSICAL CHEMISTRY C

Article

pubs.acs.org/JPCC

DFT Study of Hg Oxidation across Vanadia-Titania SCR Catalyst under Flue Gas Conditions

Ana Suarez Negreira and Jennifer Wilcox*

Departments of Chemical Engineering and Energy Resources Engineering, Stanford University, Stanford, California, 94305, United States

ABSTRACT: The density functional theory was used to analyze the thermodynamic stability and reactivity of the vanadia-titania catalyst below monolayer regime with the purpose of having a good representation of a commercial SCR catalyst (V_2O_5(<2 wt %)−TiO_2). The objective of this paper is to understand the reactivity of this catalyst in Hg oxidation. The SCR catalyst is modeled as a tetrahedrally coordinated divanadate unit supported on a 3-layer TiO_2(001) slab to represent a catalyst with low vanadia loadings. Under flue gas conditions, the interaction of water with this surface has been studied as a function of pressure and temperature using ab initio thermodynamic calculations, showing that water coverage is temperature-dependent. Adsorbed water acts as a Lewis base, donating electrons to the TiO_2(001) surface support, which increases the negative charge and reactivity of the oxygen atoms of the vanadia dimer. The reactivity of the vanadia dimer toward Hg oxidation is analyzed through the adsorption energies of Hg, HgCl, HCl, and H_2O. Surfaces with high water coverage showed higher reactivity toward HgCl, which has the highest adsorption energy, followed by HCl. The adsorption energies of Hg suggest a negligible interaction with the vanadia dimer. Lateral interactions between neighboring adsorbed flue gas components on the vanadia dimer were studied, suggesting that having H_2O or HgCl adsorbed on a neighboring oxygen atom increases the adsorption energies of Hg and HCl respectively. Temperature, pressure, and entropic effects were taken into account to study the reactivity of these surface interactions under flue gas conditions. Based on these results, it is proposed that the oxidation of Hg to $HgCl_2$ follows a Langmuir−Hinshelwood mechanism, represented as a cycle where HgCl and HCl interact without poisoning the surface. The proposed steps during the formation of $HgCl_2$ are the adsorption and dissociation of HCl, adsorption of HgCl, formation of $HgCl_2$, and its desorption from the surface.

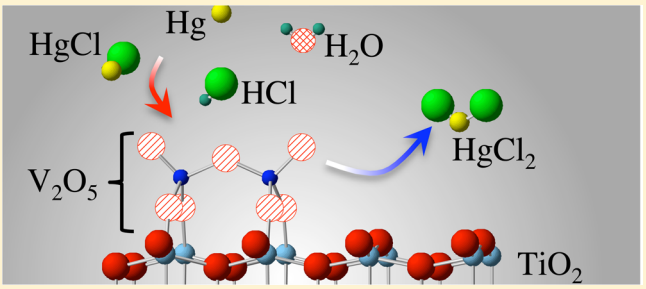

INTRODUCTION

The U.S. Environmental Protection Agency (EPA) proposed the Mercury and Air Toxics Standards (MATS) in December 2011, which require U.S. natural gas and coal-fired power plants to install air pollution control devices to prevent 91% of the Hg present in flue gas from being released.[1] Rising atmospheric levels of gaseous Hg have caused public concern because Hg has been shown to have negative neurological effects, affecting memory, attention, language, and visual skills.[2] In the U.S., 40% of the total coal-fired generating capacity is generated in power plants equipped with selective catalytic reduction (SCR) units[3] that regulate NO_x emissions with the cobenefit of Hg control[4] by oxidizing elemental mercury (Hg^0) to Hg^{2+}. Oxidized Hg is highly soluble in aqueous solutions, making its removal by conventional wet flue gas desulfurization processes possible.[5−7] A widely employed material in commercial SCR units is titania-supported vanadium and tungsten oxides, that is, V_2O_5−WO_3/TiO_2.[8,9] The active vanadia phase, V_2O_5, is responsible for NO_x reduction[10] and can also catalyze Hg^0 oxidation[11] and the undesired SO_2 to SO_3 oxidation reaction.[12] The catalysts's V_2O_5 content is limited to less than a full monolayer (<2 wt %) not only to avoid SO_3 formation, but also because high loadings of V_2O_5 decrease the temperature at which the TiO_2 anatase-to-rutile phase transformation takes place.[13] This phase transformation leads to a decrease in the surface area and the catalyst's activity.

Although mercury oxidation in the binary V_2O_5−TiO_2 system has been investigated experimentally, the detailed mechanism of this reaction is still unknown. The presence of HCl in the flue gas plays an essential role in the mercury oxidation,[5,7,14,15] but there is disagreement regarding the specific interactions between Hg, HCl, and the catalyst surface. Senior and Linjewile[7] suggest that adsorbed Hg interacts with gas-phase HCl by a Eley−Rideal mechanism, while Niksa and Fujiwara[5] suggest a Langmuir−Hinshelwood mechanism in which Hg adsorbs and then reacts with HCl that has previously been adsorbed onto the V_2O_5 surface. The kinetics governing the interaction of HCl and Hg with the surface of V_2O_5 have yet to be reported.

With respect to the TiO_2 support material, the predominant anatase (101)surface is the most stable;[16,17] however, the (001) surface is also exposed in the anatase powder that is used in

Received: October 28, 2012
Revised: December 27, 2012
Published: December 27, 2012

   dx.doi.org/10.1021/jp310668j | J. Phys. Chem. C 2013, 117, 1761−1772

commercial catalysts. This surface has been chosen for most of the theoretical work on modeling vanadia-based catalysts because of the similar geometries between the support and the active phase.[18−26] Although it is well-known that the clean (001) surface of TiO_2 undergoes a (1 × 4) reconstruction in a wide temperature range (up to 850 °C) and under a variety of experimental conditions[27−30] to decrease surface energy, water interactions with unreconstructed (001) surfaces have similar surface stabilizing effects. A study by Gong et al.[31] showed that the surface energy of TiO_2(001) decreases from 0.98 J/m^2 for the clean surface to 0.53 and 0.33 J/m^2 for dissociated water coverages of 1/3 and 1/2 monolayers (ML), respectively. The presence of unsaturated Ti atoms on the (001) surface may act as adsorption sites for H_2O through Ti−O bonding, while under-coordinated O atoms provide sites for O−H bond formation through water dissociation. The existence of hydroxyl groups on the surface of clean anatase surfaces was verified via IR spectroscopy by Topsoe et al.[32] who also showed that the intensity of the O−H peaks decreases with an increase in vanadia loading, suggesting an interaction between the vanadia and the hydroxyl groups of the support. Vittadini et al.[21] modeled hydroxylated TiO_2(001) surfaces and calculated adsorption energies for both molecular and dissociated water adsorption as a function of coverage. They showed that, for low water coverage, water tends to dissociate on the (001) surface, yielding a reconstructed surface with attached hydroxyl groups. However, when supported vanadia systems were studied by Vittadini et al.,[20] the unit cell used was small, causing vanadia dimers to cover almost the entire surface, which is not a reasonable representation of the low loading associated with SCR systems. Even for loadings higher than a theoretical V_2O_5 monolayer, only a small fraction (≈10%) of the TiO_2 surface is covered by "towers" (i.e., vertical-growth) of polycrystalline V_2O_5.[33] In addition, their surfaces contain few free surface Ti atoms, which likely exist in real systems leading to possible interactions with the water vapor present in the flue gas.

Optimal V_2O_5 loadings fall within the low coverage regime (i.e., <2 wt %), in which the disperse vanadia species are present as isolated monomeric and polymeric vanadium oxide units.[34−36] Studies of V_2O_5/TiO_2(anatase) using X-ray absorption spectroscopy (EXAFS/XANES)[37,38] indicate that, for low surface coverage, the vanadia oxide layer is characterized by isolated vanadium oxide species with the vanadium atoms having 4-fold coordination. Two different approaches have been used to model coverages of vanadia below monolayer loadings. Using a cluster-based approach the effects of the V_2O_5 cluster size and support on the reactivity of the cluster have been previously examined;[18,20,26,39,40] however, investigations employing cluster models are challenged by border effects and limited ability to investigate coverage effects. To avoid these limitations, other computational studies[22−24] have modeled this system using a periodic approach consisting of monomeric and dimeric vanadia species supported on TiO_2. These studies have focused on the stability of the vanadia species and the reactivity of the surface oxygen atoms toward NO_x reduction. Typical temperatures for NO_x reduction across the SCR unit range from 500 to 700 K.[8,9,41] However, Granite et al.[42] suggested that, for Hg oxidation, the relevant SCR temperatures are 333, 410, and 449 K, because lower temperatures favor Hg^0 adsorption,[43] which may be one step in the Hg oxidation mechanism.

In the current work, the role of the support (TiO_2(001)) and the active phase, vanadia oxide, toward Hg oxidation is investigated. Several TiO_2(001) supported submonolayer vanadia systems were tested to select a starting point for this study. The thermodynamic stability of different surfaces is investigated for temperatures ranging between 100 and 800 K, which serves as an absolute upper limit for the SCR conditions. Because the focus of this work is on flue gas conditions in which water vapor is present in significant amounts (≈10 wt %), water interactions are investigated using the unreconstructed 4 × 2 (15.18 × 7.59 Å^2) TiO_2(001) surface, with an adequate number of sites for water to interact with both the vanadia dimer and the TiO_2 support. The thermodynamic stability of different hydroxylated surfaces is studied under flue gas conditions using ab initio thermodynamic calculations. The change in the stability of the vanadia dimer with the degree of hydroxylation/hydration is also investigated through the analysis of the formation energies and the projected density of states (PDOS) of the most stable hydroxylated surfaces. Bader charge analysis is used to determine the surface charge distribution to infer the chemical reactivity by comparing the adsorption energies of the species likely playing a primary role in Hg oxidation (e.g., Hg, HCl, and HgCl). Finally, the effect of temperature and pressure on the adsorption energies of these gas-phase species is analyzed to understand the chemical nature of the SCR surface under flue gas conditions using ab initio thermodynamics. The results of this study may be used to determine the optimal conditions for Hg oxidation and provide insight into the mechanism associated with Hg oxidation across SCR catalysts.

COMPUTATIONAL METHODOLOGY

Density Functional Theory. Plane-wave DFT calculations were performed using the Vienna ab initio simulation package (VASP)[44] using the Perdew−Burke−Enzerhoff (PBE) generalized-gradient approximation (GGA).[45] For the TiO_2 bulk calculations, a projector augmented wave (PAW)[46] pseudopotential was used with an optimized energy cutoff of 500 eV. The number of k-points for the Brillion zone integration was chosen according to a Monkhorst-Pack[47] of 6 × 6 × 6 with a convergence criterion of 10^{-4} eV. The optimized lattice parameters for bulk TiO_2 (a = 3.80, b = 3.80, c = 9.55) are in reasonable agreement with experimental measurements[48] (a = 3.79, b = 3.78, c = 9.52) and previous DFT calculations (a = 3.83, b = 3.83, c = 9.62).[25]

The TiO_2 (001) surface was simulated using a 4 × 2 (15.18 × 7.59 Å^2) unit cell, without symmetry, and the inclusion of a dipole correction. The unit cell used in the current work is larger than those of previous studies[20,22] to investigate the effect of coverage in the water adsorption mode. The slabs were separated by a vacuum space of 15 Å to prevent interaction between periodic images and to cancel any dipole moment potentially created by them. A 2 × 4 × 1 k-mesh was used. The slab thickness optimization was established based upon two convergence criteria: convergence in the change of interlayer distances of the TiO_2(001) slab with respect to the bulk TiO_2, and convergence of the adsorption energies of small atoms or molecules (i.e., H, CO, NO) for slabs with increasing number of layers. These two criteria were satisfied using a 3-layer-slab, which is used in the subsequent calculations.The way in which the atomic layers are defined in the current work is shown in Figure 9 in Appendix A, along with a full description and calculations regarding the slab thickness optimization.

The lattice parameters from the bulk V_2O_5 system obtained in our previous study is used as a reference for the vanadia

dx.doi.org/10.1021/jp310668j | J. Phys. Chem. C 2013, 117, 1761−1772

species.[49] The optimized lattice parameters (a = 11.53, b = 3.58, c = 4.76) are in reasonable agreement with experimental measurements[50] (a = 11.51, b = 3.56, c = 4.37) and previous DFT calculations[51] (a = 11.65, b = 3.57, c = 4.66). Unlike a and b, their unit vector c differs more from the experimental value because we did not account for the existing van der Waals-based interlayer interaction in our DFT calculation. Gas phase molecules (H_2O, HgCl, HCl, Hg) have been calculated as isolated molecules in a 20 × 20 × 20 (Å^3) periodic box.

Ab Initio Thermodynamic Calculations. Using a procedure similar to that of our previous work,[49] ab initio thermodynamic calculations were carried out to predict the relative thermodynamic stability and composition of different terminated V_2O_5−TiO_2(001) surfaces in contact with a flue gas environment as a function of temperature and pressure. The composition of the flue gas was set to H_2O (10 wt %), HCl (4 ppm), O_2 (5 wt %), and Hg (40 ppb).[52] Mercury chloride, HgCl, is likely an intermediate species whose concentration has not been measured experimentally; however, to solve the surface free energy equation, defined below, it is necessary to define a value for its concentration. The extent of mercury oxidation across the SCR unit analyzed at different scales[7,53] varies between 20 and 60%, depending on the operating conditions. Therefore, assuming that approximately 20% of the Hg present in the flue gas oxidizes to $HgCl_2$, creating HgCl as an intermediate, a HgCl concentration of 1 ppb was chosen. This is a valid approximation because the value that enters in the surface free energy equation is the logarithm of the partial pressure of the gas species so the effect in the final surface free energy results is negligible.

The ab initio thermodynamic methodology has been explained in detail in previous studies,[49,54−58] so only the steps and explanations relevant to the current work are presented. As suggested by Rogal and Reuter,[59] when discussing the stability of phases that result from adsorbing different species simultaneously on a given surface, it is possible to refer to the cost of creating a surface with respect to the clean surface. In this way, the stability of different surfaces is evaluated based on the Gibbs free energy of adsorption, which for a semi-infinite slab with the surface in equilibrium with a gas-phase reservoir (e.g., H_2O, HCl, Hg, HgCl) at a given temperature T and pressure p is defined as

$$\Delta G^{\mathrm{ads}}(T, p) = \frac{1}{A}[G_{\mathrm{system}} - G_{\mathrm{clean}} - \sum N_i \mu_i] \quad (1)$$

where G_{system} is the Gibbs free energy of the surface covered with any adsorbates, G_{clean} is the Gibbs free energy of the corresponding clean surface, N_i is the number of gas phase species, and μ_i is the chemical potential of these gas phase species (μH_2O, μHCl, μHgCl, μHg). The Gibbs free energy terms in eq 1 are defined as $G = E_{\mathrm{total}} + F^{\mathrm{vib}} + F^{\mathrm{conf}} + pV$. Previous DFT studies[56,59−61] consider that, for any p < 100 atm and any T < 1000 K, the contributions from pressure (pV) and configurational free energy (F^{conf}) may be neglected. Rogal and Reuter[59] also suggested that vibrational free energies of the solid bulk and surface cancel each other so that only the vibrational contribution from the adsorbed species requires consideration. In the current system, the differences in the vibrations associated with the vanadia dimers in G_{system} and G_{clean} differ less than 10 meV/Å^2 for any T < 1000 K, falling within the accuracy of the DFT predictions,[62] and they were therefore not included in the surface free energy calculations. However, as reported by Sum et al.,[62] the vibrational contributions of adsorbed hydroxyl and water functional groups to the surface free energy is not negligible and it needs to be included. In the current study, the vibrational free energies of the adsorbed hydroxyl and water groups are calculated using the harmonic oscillator approximation[59] and presented in Figure 10 in Appendix B.

The chemical potential of the system components are temperature- and pressure-dependent,[59] as can be seen from eq 2.

$$\mu_i(T, p) = E_i^{\mathrm{tot}}(\mathrm{DFT}) + E_i^{\mathrm{ZPE}} + \mu_i(T, p^0) + k_B T \ln\left(\frac{p_i}{p^0}\right) \quad (2)$$

where $\mu_i(T, p_0)$ can be obtained from the NIST-JANAF thermochemical tables at standard pressure p_0, 1 atm;[63] E_i^{ZPE} arises from the zero-point vibrations and E_i^{tot} is the total energy. This relationship only holds for a surface in equilibrium with a gas-phase environment. Therefore, it is necessary to establish physical limits to confirm these gas-phase conditions. The upper limit for the chemical potential of water vapor is μH_2O = −0.91 eV, which corresponds to the critical point of water,[62] and the flue gas conditions of interest are within this limit. The final equation to calculate the Gibbs free energy of adsorption as a function of pressure and temperature is

$$\Delta G^{\mathrm{ads}}(T, p) = \frac{1}{A}[E_{\mathrm{syst}} - E_{\mathrm{clean}} + \Delta F^{\mathrm{vib}}_{H_{\mathrm{ad}}} - N_{H_2O}\mu_{H_2O} - N_{\mathrm{HCl}}\mu_{\mathrm{HCl}} - N_{\mathrm{HgCl}}\mu_{\mathrm{HgCl}} - N_{\mathrm{Hg}}\mu_{\mathrm{Hg}}] \quad (3)$$

RESULTS

Modeling TiO_2(001)-Supported Vanadia Oxide Species. Vanadia species are present on the surface as monomeric and polymeric structures in the low loading regime (i.e., <2 wt %). The advantage of using dimeric species is the possibility of modeling the active sites that participate in the catalytic activity, that is, vanadyl O (V=O(1)) and bridging O (V−O(2)−V),[24] as shown in Figure 1. To represent vanadia species below monolayer coverage, dimeric vanadia species were chosen, similar to Vittadini et al.[20] to model the simplest polyvanadate structure with two adjacent metal sites in tetra-coordinated-O environments. Due to the reconstruction of the TiO_2(001) surface, the support in Vittadini's vanadia dimer system follows the so-called "ad-molecule" (ADM) model, which requires a (1 × 4) unit cell.[64] However, a larger and more computational expensive unit cell would be required to model the interaction of water molecules with both the support and the isolated vanadia dimer, which is the purpose of the current study. To be able to use a small unit cell but still account for the surface reconstruction, Vittadini et al.[20] approximated the energy of the ADM model by adding the reconstruction energy to the energy of a (1 × 1)-unreconstructed-(2 × 2)TiO_2(001) slab. Following this procedure, the isolated vanadia dimer supported on a (4 × 2)-unreconstructed-TiO_2(001) surface was modeled, adding the reconstruction energy during the stability analysis. The reconstruction energy is calculated as the difference between the surface energies of (1 × 1)-unreconstructed and (1 × 4)-reconstructed TiO_2(001) slabs, which are 0.124 and 0.098 eV/Å^2, respectively.

The stability analysis allows us to establish the starting vanadia−titania structure. Three possible dimeric structures are shown in Figure 1, differing only in the orientation of the V−

dx.doi.org/10.1021/jp310668j | J. Phys. Chem. C 2013, 117, 1761−1772

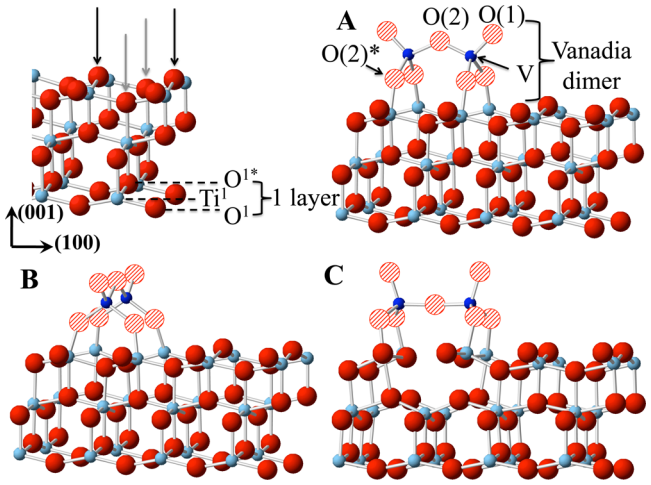

Figure 1. Clean surface and three possible configurations of the vanadia dimers. Dark blue atoms are V, red atoms are O from the support, striped red atoms are O atoms from vanadia dimer, and light blue atoms are Ti. Black arrows indicate the O atoms that are missing in structures A and B, while gray arrows indicate the O atoms missing in structure C.

O(2)−V bond and the missing surface oxygen atoms. Of these three systems, structure A is chosed as the structure used in the subsequent calculations due to its lowest formation energy and the smallest change in the interlayer distance with respect structure B and C. A full description of the formation energy calculations and the change in the interlayer distances for these three structures are presented in the Appendix C.

Interaction with H_2O. The interaction with H_2O is done in the (4 × 2)-unreconstructed (15.18 × 7.59 Å^2), which has four unique Ti atoms that water may interact with molecularly (Mol), dissociatively (Dis), or via some combination (Mix). As was indicated by Vittadini et al.,[21] at low water coverage dissociation is favored because it decreases the surface energy of the system due to surface reconstruction.[31] This surface reconstruction upon water dissociation is shown in Figure 2.

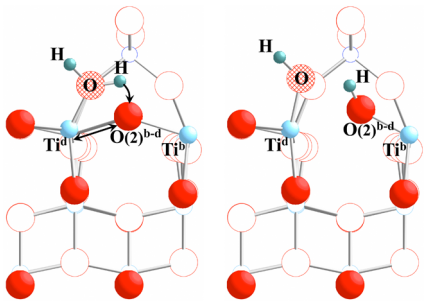

Figure 2. Surface reconstruction taking place during water dissociation on the Ti surface atoms of structure A.

Water originally adsorbs on the Ti^d atom, with one of the H atoms interacting with a neighboring O(2) atom, leading to the stretching and finally cleavage of the Ti^d−O(2) bond. This action produces two hydroxylated Ti atoms, that is, HO−Ti^d and H−O(2)−Ti^b. Because the adsorption and dissociation of one water molecule leads to the hydroxylation of two Ti atoms, this coverage is considered as θ = 0.5. The different configurations for water adsorption/dissociation for each of the coverages tested are summarized in Table 1. The atoms that participate in the water adsorption/dissociation are indicated in Figure 3, where examples of dissociative and molecular water adsorption are also illustrated.

The thermodynamic stability of the different hydroxylated and hydrated surfaces was calculated using eq 3 as a function of temperature, yielding a straight line for each surface. The surface associated with the lowest-lying line corresponds to the most stable structure under the given flue gas conditions. For simplicity, only the structures with the lowest Gibbs free energies of adsorption are shown in Figure 4, while all the others are presented in Figure 11 in the Appendix D.

In Figure 4, the different stable regions are separated by red-dashed vertical lines at 100, 150, 240, and 390 K. The most stable surface in each region is illustrated in Figure 5 where the evolution of surface hydroxylation/hydroxylation with temperature can be seen. The first region corresponds to temperatures below 100 K, where, due to the high water vapor concentration in the flue gas and the low temperature, water molecules interact with all Ti and V−O(2) atoms on the surface. As the temperature increases, water desorbs from the vanadia dimer. This indicates that water interacts more strongly with the undercoordinated Ti atoms of the support than with the vanadia dimer. This result differs from the prediction of Calatayud and Minot,[24] who suggested that V_2O_5 units are hydroxylated before the TiO_2(001) support based on their investigation of H interactions with the supported system. Between 150 and 240 K, water molecules begin desorbing from the support, leaving room for water dissociation to take place. For this reason, the most stable structure in this region is Mix-1, in which both molecular and dissociative water molecules coexist on the surface. As the water coverage decreases, the dissociative adsorption mode becomes more stable, in agreement with previous theoretical[21] and experimental[65] studies. Above 390 K, water completely desorbs from the surface, leading to the clean surface, A.

Comparing the results of the current work with previous studies is difficult due to the differences in model systems and theoretical approaches used in the various studies. Vittadini et al.[21] studied the interaction of water with the unreconstructed (1 × 1)-TiO_2(001) surface obtaining adsorption energies of −1.44 eV for the dissociative case and −0.81 eV for the molecular case, for a water coverage of 1/2 ML. For the same coverage conditions in the current system, adsorption energies of −1.24 eV for the dissociative case and −0.84 eV for the molecular case were obtained. The difference in the adsorption energies may be due to the presence of the vanadia dimer, which was shown to change the geometry of the support. Also, lateral interactions between water molecules and the vanadia dimer may affect water adsorption. The interaction of water with the surface may be further studied through the analysis of density of states, DOS, which is shown in Figure 12 in the Appendix E.

The surface reactivity of the most stable hydroxylated surfaces for T > 150 K (Mix-1, Dis-3 and A) are analyzed by Bader charge analysis to determine the charge distribution during the dehydroxylation process. An attempt to correlate the atomic charge of the surface atoms of the vanadia dimer with their reactivity toward the gas species likely playing a role in Hg oxidation, for example, Hg, HCl, and HgCl, was made as a first step in understanding the reaction mechanism.

Bader Charge Analysis. In this work, the Bader charge analysis is used to determine the electronic changes associated with the dehydration process. The atomic charges for the

dx.doi.org/10.1021/jp310668j | J. Phys. Chem. C 2013, 117, 1761−1772

Table 1. All Molecularly and Dissociative Water Adsorption Configurations at Different Coverages[a]

structure	coverage	Ti^a	Ti^c	Ti^b	Ti^d	$O(2)^{a-c}$	$O(2)^{b-d}$	V−O−V
A	0							
Dis-1	0.5		OH			H		
Dis-2	0.5				OH		H	
Dis-3	1		OH		OH	H	H	
Mol-1	0.25		H_2O					
Mol-2	0.25			H_2O				
Mol-3	0.5		H_2O	H_2O				
Mol-4	0.75		H_2O	H_2O	H_2O			
Mol-5	1	H_2O	H_2O	H_2O	H_2O			
Mol-6	1	H_2O	H_2O	H_2O	H_2O			H_2O
Mol-7	0							H_2O
Mix-1	1		OH	H_2O	H_2O	H		
Mix-2	0.75		OH	H_2O	H			
Mix-3	1		OH	H_2O	H_2O	H		H_2O

[a]For water dissociation, adsorption sites for both the −OH and the -H functional groups are indicated.

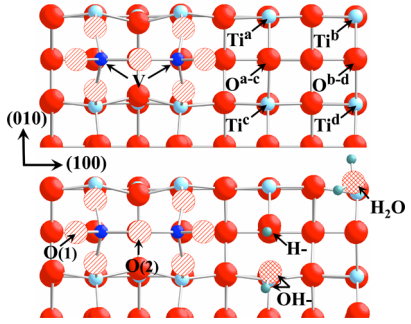

Figure 3. Upper figure represents surface A and four possible Ti surface atoms where water may interact. Lower figure shows the two adsorption modes, dissociative (H−OH) and molecularly (H_2O). The water molecule is represented as red-hatched O atoms and small gray H atoms.

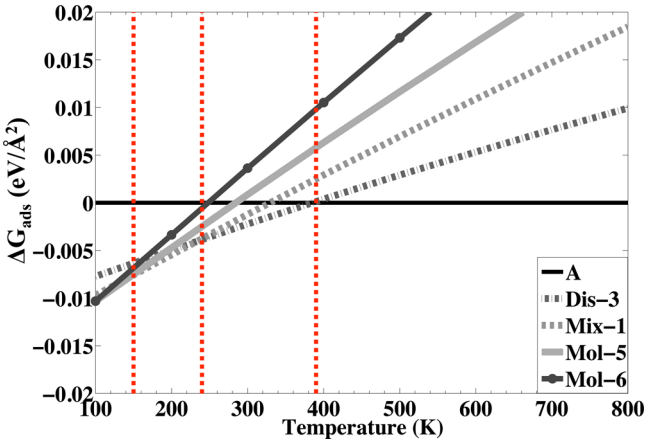

Figure 4. Gibbs free energy of adsorption plot for surfaces in equilibrium with flue gas environment. Red-dashed vertical lines indicate a transition between adsorbate systems (H_2O terminated surfaces) with the most negative Gibbs free energy of adsorption as a function of temperature.

different surface atoms (labeled in Figure 6 for clarity) of the Mix-1, Dis-3, and A surfaces are summarized in Table 2.

Table 2 shows that water donates electrons to the support, behaving as a Lewis base. As the number of adsorbed water molecules increases from A to Dis-3 to Mix-1, the charge on each of the three vanadia dimer oxygen atoms becomes more

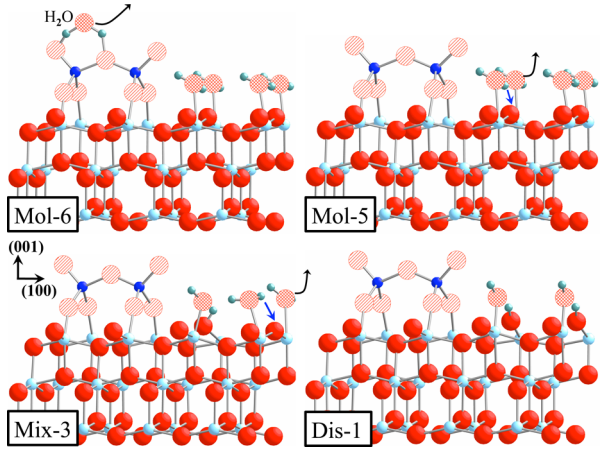

Figure 5. Evolution of surface hydroxylation/hydroxylation with temperature. The water molecule is represented as red-hatched O atoms and small gray H atoms. Black arrows indicate water molecules leaving the surface. Blue arrows indicate water dissociation.

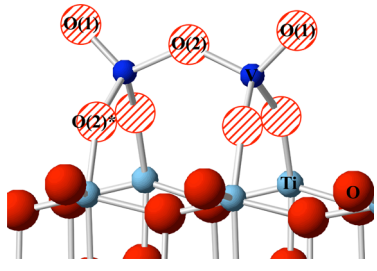

Figure 6. Dark blue atoms are V, red atoms are O from the support, striped red atoms are O atoms from vanadia dimer, and light blue atoms are Ti atoms.

Table 2. Summary of Atomic Charge of the Oxygen Atoms of the Vanadia Dimer as a Function of Hydroxylation/Hydration

surface atom	Mix-1 (150−240 K)	Dis-3 (240−390 K)	A (>390 K)
O(1)−V	−0.66	−0.62	−0.59
O(2)	−0.88	−0.90	−0.88
O(2)*−V	−0.89	−0.88	−0.88

dx.doi.org/10.1021/jp310668j | J. Phys. Chem. C 2013, 117, 1761−1772

negative. This effect is most significant for the O(1) atoms, that is, the first row of Table 2. This increase in the charge transfer between the hydroxylated support and vanadia dimer may yield a stronger dimer−support interaction. This increase in the stability of the vanadia dimer as a function of water adsorption was verified through the analysis of the formation energies and the PDOS of the different hydroxylated/hydrated surfaces, and it is shown in Table 7 and Figure 13 in Appendix F.

In the next section, these changes in the electronic structure of the three most stable surfaces for $T > 100$ K (Mix-1, Dis-3, and A) are linked with the change in reactivity of the vanadia dimer by analyzing the interaction with gas species Hg, HCl, and HgCl.

Reactive Sites: Adsorption Energies of Hg, HgCl, and HCl. Elucidating the mechanism of Hg oxidation requires analyzing the adsorption energies of Hg, HgCl, and HCl species, which are likely involved in the oxidation mechanism. Because the ab initio thermodynamic results suggest that the degree of hydroxylation/hydration of the surface changes with temperature within the working conditions of the SCR unit, we examine the interaction of Hg, HgCl, and HCl with the most stable surface under those conditions, that is, Mix-1 (150−240 K), Dis-3 (240−390 K), and A (>390 K), which are shown in Figure 5. The adsorption energies of Hg, HgCl, and HCl at different adsorption sites are summarized in Table 3. The adsorption sites chosen in this work are the surface oxygen atoms of the vanadia dimer are labeled in Figure 6.

Table 3. Adsorption Energies (eV) of Hg, HgCl, and HCl Molecules on Different Surface Oxygen Atoms of the Most Stable Surface for $T > 100$ K[a]

gas phase	adsorption mode	Mix-1 (150−240 K)	Dis-3 (240−390 K)	A (> 390 K)
	O(1)−Hg	−0.039	−0.006	0.947
Hg	O(2)−Hg	−0.028	−0.005	0.941
	O(1)−HgCl	−0.744	−0.776	0.019
HgCl	O(2)−HgCl	−0.223	−0.234	0.675
	O(1)−HCl	−0.203	−0.146	0.792
HCl	O(2)−HCl	−0.093	−0.071	0.885
	O(1)−Cl/ O(1)−H	1.626	1.664	2.546
	O(2)−Cl/ O(1)−H	ND	ND	ND

[a]The cases in which HCl dissociative adsorption does not occur are indicated by "ND", which stands for "no dissociation".

From the results shown in Table 3, two factors will be analyzed that affect the adsorption energy: the nature of the gas species and the degree of hydroxylation/hydration of the surface. The adsorption energies are correlated with the results of the Bader charge analysis for increased understanding of the changes that take place in the electronic structure upon hydroxylation.

Nature of the Gas Species. A comparison of the adsorption energies among the three species indicates that HgCl has the highest affinity for the surface. The two HgCl orientations tested differ by which atom, Hg or Cl, was interacting directly with the surface. The configuration in which the chlorine atom is singly coordinated, that is, Cl−Hg-surface, was energetically favored. Because HgCl is a radical species, it is not expected to be stable in the gas phase, but rather is likely to exist as a surface-bound intermediate, as indicated by previous studies on Hg adsorption across carbon surfaces.[66,67] This intermediate species may also exist to some extent in the gas phase[68−70] at elevated temperatures and may react with surface-adsorbed Cl atoms to form $HgCl_2$ or adsorb on the surface prior to reaction with a gas-phase $Cl^{\bullet}$ radical to form $HgCl_2$.

It is well-known that Hg is stable in the gas phase of coal-fired flue gas and as such has the lowest adsorption energies of all of the adsorbates investigated. It has been suggested[7,14,15] that Hg is displaced on the surface by HCl when both gases are injected in the flue gas. Our results agree with these experimental findings, because lower adsorption energies were obtained for Hg compared to HCl. Mercury acts as a Lewis base prior to oxidation, thereby is likely to react with electron-deficient species.[67] As the Bader analysis revealed, all of the surface oxygen atoms are negatively charged and therefore have a low affinity for Hg atoms.

The interaction of HCl with the surface was also investigated based upon two orientations. Again, the configuration in which the chlorine atom is singly coordinated, that is, Cl−H-surface, was energetically favored. The HCl interaction was also studied in a molecular and dissociative manner. The dissociation of HCl was analyzed by investigating the potential bonding of H and Cl atoms with one of the surface oxygen atoms (O(1) or O(2)). When dissociation is tested by placing H and Cl atoms on both the O(1) atoms of the vanadia dimer, the optimized final configuration is not energetically favored, that is, resulting in positive adsorption energies. If the H and Cl atoms are placed closer on the surface, that is, Cl interacting with the bridging O(2) atom and the H atom interacting with the O(1) atom, this leads to an optimized final configuration in which the Cl atom moves away from the surface, interacting directly with the H atom in a molecular mode, so dissociation does not take place (labeled as "ND" in Table 3).

Degree of Hydroxylation. From left to right in each row of Table 3, it can be seen that the adsorption energies decrease, some of them even becoming thermodynamically unfavorable, as the degree of hydroxylation decreases. The strongest adsorption energies take place on the Mix-1 surface, which has the highest degree of hydroxylation of the three surfaces. This may be due to the increased concentration of negatively charged O atoms on the Mix-1 surface. However, negative charge is not the only factor influencing the strength of adsorption since the O(2) atom is more negative than the O(1) atom in all of the surfaces yet does not necessarily indicate higher reactivity. Steric effects associated with the more constrained location of the bridging O(2) atom may also be responsible for the smaller adsorption energies for this atom.

Up to this point, only the adsorption of single species (Hg, HgCl, or HCl) on different oxygen atoms of the supported vanadia dimer have been of focus. To account for lateral interactions, simultaneous adsorption of multiple flue gas species on the oxygen atoms of the supported vanadia dimer was carried out on the three most stable hydroxylated surfaces (Mix-1, Dis-3, and A). From the adsorption study of single components, it was shown that O(1) was the most reactive oxygen atom in the vanadia dimer. The study of simultaneous adsorption will be limited to the adsorption of different combinations of Hg, HCl, HgCl, and H_2O on the two O(1) sites of the vanadia dimer. The adsorption energies are calculated using eqs 4 and 5 and the energies are summarized in Table 4.

$$E_{ad} = E_{Hg-X} - (E_X + E_{Hg}^{gas}) \quad (4)$$

dx.doi.org/10.1021/jp310668j | J. Phys. Chem. C 2013, 117, 1761−1772

Table 4. Change in the Adsorption Energy of Either Hg or HCl Adsorbed on the O(1) Oxygen Atom Due to Lateral Interactions of a Coadsorbed Gas Species X (X = H_2O, HCl, Hg, and HgCl) on the Neighboring O(1) Oxygen Atom

Hg-X	Mix-1	Dis-3	A	HCl-X	Mix-1	Dis-3	A
empty	−0.039	−0.006	0.921	empty	−0.203	−0.146	0.729
HCl	−0.014	−0.002	0.000	Hg	−0.166	−0.144	−0.123
H_2O	−0.104	−0.022	−0.057	H_2O	−0.252	−0.097	−0.085
HgCl	−0.012	−0.014	−0.009	HgCl	−0.245	−0.233	−0.223
Hg	−0.035	−0.004	0.457	HCl	−0.173	−0.124	0.360

$$E_{ad} = E_{HCl-X} - (E_X + E_{HCl}^{gas}) \quad (5)$$

where E_{Hg-X} and E_{HCl-X} are the energies of the surface (Mix-1, Dis-3, or A) with either Hg or HCl adsorbed onto one of the O(1) atom and X adsorbed on the other O(1) atom (X = HCl, Hg, H_2O, or HgCl), E_X is the energy of the surface, with X adsorbed on one O(1) atom, and E_{Hg}^{gas} and E_{HCl}^{gas} are the energies of the Hg and HCl in gas.

In general, changes in the adsorption energies smaller than 0.01 eV/atom may be considered negligible because they are within the calculation error of VASP. From Table 4 it is possible to see that lateral interactions due to a neighboring adsorbate increases the adsorption energies of both Hg and HCl on the water free surface (surface A), independently of the nature of the second adsorbate. Water adsorbed on a neighboring O(1) atom increases the adsorption energies of Hg and HCl on surfaces Mix-1 and A, but decreases the energy for surface Dis-3. Having HCl, HgCl, or a second Hg atom adsorbed on a neighboring O(1) atom either slightly decreases or has a negligible effect on the adsorption energies of Hg. As for the adsorption of HCl, Hg has a negligible effect on the hydroxylated supported system while it increases the HCl adsorption energy in the case of the water free surface. The strongest effect on HCl adsorption is due to a neighboring adsorbed HgCl compound, which increases the HCl adsorption energy suggesting a strong cooperative effect. The effect of temperature and pressure on the adsorption energies of both single and multiple adsorbate interactions are studied in the next section, and those results are then used to propose a mechanism for the Hg oxidation.

Ab Initio Thermodynamics for Hg, HgCl, and HCl Terminated Surfaces. Adsorption energies presented in Tables 3 and 4 have been calculated with DFT values obtained at 0 K and therefore they are not indicative of the change in adsorption energies with temperature. Ab initio thermodynamic calculations were carried out to include the effect of the temperature and pressure on the adsorption energies of Hg, HgCl, HCl, H_2O, and their combinations. In this way, the entropic effects are being taken into account, which become important at high temperatures. More than 30 surfaces were tested, but for simplicity, only the most stable surfaces are presented in this section. The most stable surfaces correspond to those where flue gas species interact with the O(1) atoms, as was shown in Table 4, in which both Hg and H_2O and HgCl and HCl were simultaneously adsorbed on O(1) sites. The changes in the Gibbs free energy of adsorption of these surfaces as a function of temperature are shown in Figure 7.

Figure 7 shows the decrease in the adsorption energies of Hg, HgCl, HCl, H_2O and their combinations with increasing temperature. At higher temperatures, the entropy loss during adsorption overcomes the adsorption energy, breaking the surface−adsorbate bond. At low temperatures, the surfaces with both HgCl and HCl adsorbed (magenta lines) on the three

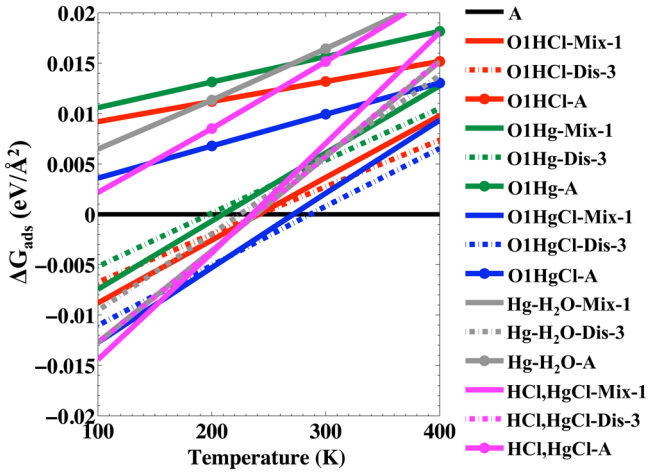

Figure 7. Temperature dependence of the adsorption energies of Hg, HgCl, HCl, and their combinations on three most stable surfaces for T > 100 K (Mix-1, Dis-3, and A).

hydroxylated surfaces are the most energetically favored, while Hg interactions (green lines) have the lowest adsorption energies. The adsorption energy lines of the individual Hg, HgCl and HCl adsorbed on the surfaces Mix-1 and Dis-3 cross between 220 and 250 K, which may be due to the transition between Mix-1 and Dis-3 surfaces at 240 K, as shown in Figure 4.

These ab initio results indicate that, in the limit of thermodynamic equilibrium, the adsorption of Hg, HCl, HgCl, and their combinations are not energetically favored for T > 300 K, suggesting that poisoning of our surface catalyst under flue gas conditions is not expected. The Sabatier principle indicates that the ideal catalyst lies in a region of trade-off between weakly adsorbing reactant species and easily desorbing products to avoid the poisoning of the active sites. The same reasoning was employed by Jones et al.[71] to select suitable catalysts for the steam reforming reaction. These thermodynamic results may be used as a basis to begin kinetic modeling in order to completely understand the reactivity of the current system toward Hg oxidation. Investigation of the relatively stable surface species provides an indication of the likely intermediates playing a role in the Hg oxidation pathway. Based on the adsorption energies shown in Tables 3 and 4 and the results in Figure 7, it can be seen that HCl and HgCl adsorb stronger than Hg, and that HgCl has a cooperative effect on the HCl adsorption, such that these two species may interact simultaneously on the surface. Based on these results, the mechanism of Hg oxidation through the formation of $HgCl_2$ is proposed in Figure 8.

The proposed oxidation mechanism represents a cycle where HgCl and HCl interacts without poisoning the surface, since the original catalyst is the first and last step of the reaction. The proposed Hg oxidation mechanism may involve the following

dx.doi.org/10.1021/jp310668j | J. Phys. Chem. C 2013, 117, 1761−1772

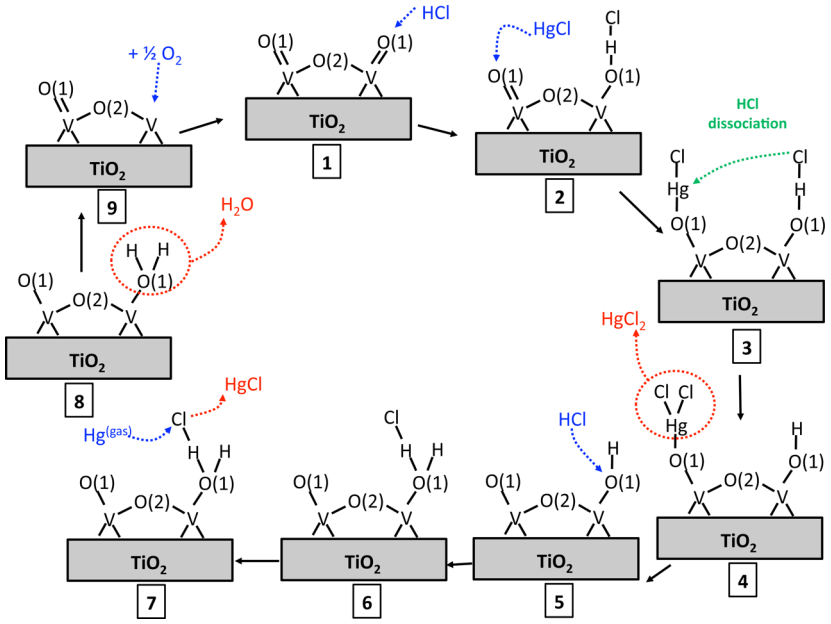

Figure 8. Proposed mechanism of mercury oxidation on vanadia-titania SCR catalyst. Blue arrows indicate an adsorption step, green arrows indicate a dissociation step, and red arrows indicate a desorption step.

steps: the adsorption of HCl (steps 1 and 5) and adsorption of HgCl (step 2) on the surface, following a Langmuir–Hinshelwood mechanism. The dissociation of adsorbed HCl (steps 3) occurs due to the stretching of the H–Cl bond that takes place during the interaction of the Cl atom with the Hg atom from HgCl to form $HgCl_2$ (steps 3 and 4). Three products are formed and desorbed from the surface in this cycle, HgCl (step 7), $HgCl_2$ (step 4), and H_2O (step 8). Due to the weak Hg adsorption energies, it is proposed that HgCl is formed following an Eley–Rideal mechanism where gas phase Hg interacts with adsorbed HCl. An oxygen vacancy may be created (step 8) during water desorption, but it is likely that it is replenished due to the presence of oxygen in flue gas.

The previously proposed Hg oxidation mechanism involving an Eley–Rideal mechanism,[7] where Hg adsorbs on the surface followed by an interaction with gas phase HCl, should not be ignored. An analysis of the activation barriers associated with each step of both mechanisms is necessary in order to discard one of them. A Langmuir–Hinshelwood mechanism is proposed due to the stronger HCl and HgCl interaction with the surface, and the higher concentration of HCl in the gas phase compared to Hg, which both make step 1 more probable than the interaction of the surface with Hg. Future work will focus on building the kinetic model, where a wider range of possible reactions paths will be considered, so it may be possible to establish rate-determining steps and activation energies involved in Hg oxidation, which could validate the proposed mechanism.

CONCLUSIONS

With the purpose of having a good representation of a commercial SCR catalyst (V_2O_5(<2 wt %)–TiO_2) whose vanadia content falls below the monolayer regime, the active phase was modeled as a vanadia dimer supported on a 3-layer TiO_2(001) slab. This model allows us to study the active sites that participate in the catalytic activity: vanadyl oxygen (V=O(1)) and bridging O (V–O(2)–V). The significant concentration of water vapor present in the flue gas (≈10%) and the stabilization effect that water has on the TiO_2(001) surface led us to study the thermodynamic stability of different hydrated and hydroxylated surfaces as a function of pressure and temperature. In agreement with previous experimental and theoretical work, it was shown that water interacts in a molecular or in a dissociative fashion depending on the water coverage, which is temperature dependent. A dehydration process takes places with increasing temperatures leading to a water free surface above 390 K.

The reactivity of the vanadia dimer is analyzed through the adsorption energies of Hg, HgCl, HCl, H_2O, and their combinations, which are likely involved in the Hg oxidation mechanism. These adsorption energies are correlated with the results of the Bader charge analysis and PDOS of the vanadia dimer for increased understanding of the changes in the electronic structure upon dehydration. In the first part of the reactivity analysis, temperature and pressure effects are not taken into account to understand the individual effect of hydroxylation on the adsorption energies, calculated at 0 K. It was observed that adsorbed water acts a Lewis base, donating electrons to the support, which increases the negative charge on the oxygen atoms of the vanadia dimer. This increase in charge leads to higher reactivity of those oxygen atoms and a stronger vanadia–titania interaction. The surface with high water coverage showed higher reactivity toward HgCl, which has the highest adsorption energy, followed by HCl. The adsorption energies of Hg suggest a weak interaction with the vanadia dimer only on surfaces with high water coverage.

In the second part of the reactivity analysis, ab initio thermodynamic calculations were carried out to take into account the effect of temperature and entropy loss on the adsorption energies of Hg, HgCl, HCl, and H_2O and their combinations. Adsorption energies of these species decrease with increasing temperatures, becoming energetically unfavorable at $T > 300$ K. A mechanism to explain Hg oxidation has been proposed based on the adsorption energies calculated at 300 K. This mechanism may involve the adsorption of HCl and HgCl, following a Langmuir–Hinshelwood mechanism. The

dx.doi.org/10.1021/jp310668j | J. Phys. Chem. C 2013, 117, 1761–1772

oxidation of Hg to $HgCl_2$ is represented as a cycle, where HgCl and HCl interact without poisoning the surface, since the original catalyst is the first and last step of the reaction. Some of the steps during the formation of $HgCl_2$ may include adsorption and dissociation of HCl, adsorption of HgCl, formation of $HgCl_2$, and its desorption from the surface.

Because the active vanadia phase, V_2O_5, is responsible for NO_x reduction and the undesired SO_2 to SO_3 oxidation reaction, the impact of other flue gas components, such as sulfur dioxide (SO_2), sulfur trioxide (SO_3), nitrogen monoxide (NO), and nitrogen dioxide (NO_2), on mercury oxidation across the SCR unit will also be examined in future work. These results from DFT may aid in the design of improved catalysts for mercury oxidation while simultaneously maintaining optimal performance for NO_x reduction.

APPENDIX

Appendix A: Modeling the TiO_2(001) Support

The TiO_2(001) surface has been studied previously,[16,25,30,72] and is shown in Figure 9. It is composed of five-coordinated Ti

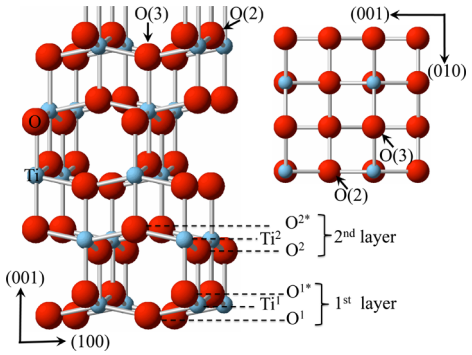

Figure 9. Bulk TiO_2.

atoms bonded to two O atoms along the (001) direction and to three O atoms in the (010) direction. In the TiO_2 bulk structure, the bond distances between the Ti and O atoms from the upper and lower layer, in the (001) direction, are identical (i.e., in bulk, the atomic distance, Ti^2-O^3, equals the atomic distance, Ti^2-O^{1*}, as shown in Figure 9. However, in the case of the slab calculations, the atomic distances are different since the 1st layer (i.e., bottom layer) is fixed to the bulk parameters, while the surface is unconstrained. For this reason, the interlayer distance is defined as the average distance between Ti^x-O^{x+1} and Ti^x-O^{x-1*}, where x is defined as the layer number counted from the bottom of the slab. The way in which the atomic layers are defined in the current work is shown in Figure 9.

In general, larger models are preferred for representing real systems, but the computational cost increases with size. To balance computational time and accuracy, the optimal slab thickness was established based upon two convergence criteria: convergence in the change of interlayer distances of the TiO_2(001) slab with respect to the bulk and convergence of the adsorption energies of small atoms or molecules (i.e., H, CO, NO).

The change in the interlayer distances with respect to the optimized TiO_2 bulk structure as the system is allowed to relax was compared for slabs with increasing number of layers. Accuracy is reached when the inner layer distance does not change with respect to the bulk configuration. The inner-layer spacings of the bulk, 3-layer, 4-layer, and 5-layer slabs, and percent difference were calculated and negligible changes (<1.5%) were obtained for all cases considered. Similar changes in the bond distances were obtained by Calatayud and Minot,[23] who also modeled the TiO_2(001) surface as a 3-layer slab with a fixed bottom layer.

The other parameter validated during the slab optimization is the change in the adsorption energies of small atoms or molecules (i.e., H, CO, NO) with increasing number of layers. The convergence criterion for adsorption energies is reached if the change of the adsorption energy with respect to the 5-layer slab is within 0.01 eV/atom. The adsorption energies are calculated using eq 6:

$$E_{ad}^{x} = E_{system} - (E_{x}^{gas-phase} + E_{clean}) \quad (6)$$

where E_{system}, $E_x^{gas\text{-}phase}$, and E_{clean} are the calculated energies of the surface after adsorption of X atom/molecule, the energy of X in the gas phase and the energy of the clean surface prior to adsorption, respectively. As is shown in Table 5, convergence in

Table 5. Layer Optimization

No. of layer	E_{ad}^{H} (eV)	E_{ad}^{CO} (eV)	E_{ad}^{NO} (eV)
2	−2.25	0.02	−1.98
3	−2.48	−0.04	−2.37
4	−2.46	−0.04	−2.23
5	−2.46	−0.04	−2.36

the adsorption energies for CO and NO is achieved using a 3-layer slab with the bottom layer fixed to the bulk parameters. Although convergence in the adsorption energy of H is not reached until the use of a 4-layer slab, the lower computational cost and negligible changes in the inner-layer spacing collectively justify the use of the 3-layer slab.

Appendix B: Vibrational Contributions of the Surface Hydroxyl and Water Groups

The vibrational frequency contribution sourced from the adsorbed hydroxyl and water functional groups, ΔF_H^{vib-ad}, was calculated to understand its contribution to the total Gibbs free energy. In the current study the vibrational free energies of the adsorbed hydroxyl and water groups are calculated using the harmonic oscillator approximation as[59]

$$F_{H_{ad}}^{vib} = \sum_{k}^{3N}\left[\frac{h\omega_k}{2} + k_B T \ln(1 - e^{h\omega_k/k_B T})\right] \quad (7)$$

in which the sum is over the vibrational modes, ω_K, of each of the N adsorbed atoms. The vibrational contribution of each surface is shown in Figure 10 and was calculated by diagonalizing the complete dynamic matrix while leaving the substrate fixed.[73] The line colors represent a different number of water molecules, molecularly and dissociatively adsorbed. It can be seen that the vibrational contribution increases with increasing number of water molecules interacting with the surface. At temperatures below 600 K, the mechanism by which water is adsorbed does not significantly influence the vibrational contribution, although dissociated water molecules provide a smaller contribution than molecularly absorbed water molecules at temperatures above 600 K.

Appendix C: Modeling TiO_2(001)-Supported Vanadia Oxide Species

Three possible dimeric structures are shown in Figure 1, differing only in the orientation of the V−O(2)−V bond and

dx.doi.org/10.1021/jp310668j | J. Phys. Chem. C 2013, 117, 1761−1772

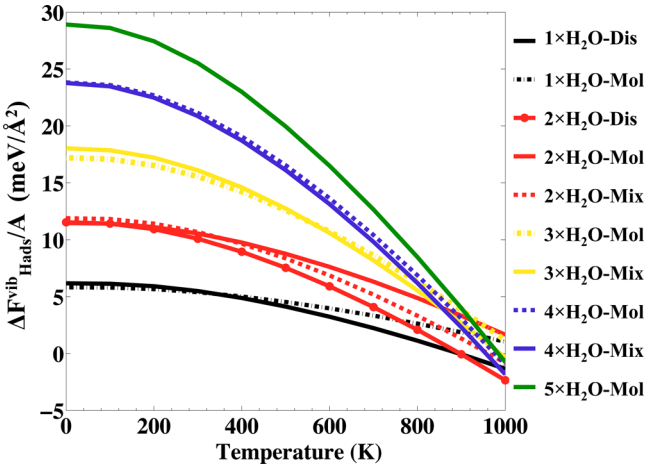

Figure 10. Vibrational contribution of surface hydrogen groups (−H, H_2O, and −OH) to the surface free energy of different hydroxylated and hydrated (vanadia-TiO_2) surfaces.

the missing surface oxygen atoms. Both structures A and C have a V−O(2)−V bond lying in the (100) direction, but they differ in their missing surface oxygen atom. Structure A is missing the O atoms indicated with black arrows in Figure 1, while structure C is missing the O atoms indicated with grey arrows. In the case of structure B, the V−O(2)−V bond follows the (010) direction with the missing O atoms corresponding to those indicated by black arrows. Following the procedure used by Vittadini et al.,[20] the relative stability of each vanadia structure was analyzed based on the formation energies, using the (1 × 4)-reconstructed TiO_2(001) and V_2O_5 bulk, $E_{nVO_{2.5}}$, phase as references. The energy of the former is obtained by adding the reconstruction energy, E_{recon} to the energy of the (1 × 1)-unreconstructed (4 × 2) TiO_2(001) slab, E_{uncon}. The formation energy, E_{form}, is defined as

$$E_{form} = E_{uncon} - [E_{nVO_{2.5}} + E_{TiO_2} + E_{recon}] \quad (8)$$

The formation energies are −0.33, 0.75, and 3.49 eV for structures A, B, and C, respectively. Structure A is the most stable dimer configuration, and it is equivalent to structure D1, the most stable dimer structure in Vittadini et al.[20] They suggested that the structural similarity between D1 and the (1 × 4)-reconstructed TiO_2(001) explain the higher stability of D1 surface. The interaction of the vanadia dimer with the support leads to a geometry distortion of the later. The changes in the inner layer distances measured with respect the 3-layer-unreconstructed TiO_2(001) slab are shown in Table 6.

Structure A has the smallest interlayer change, with expansion of the middle and top layers of 0.26 and 1.62% (Å) in the (001) direction, respectively. The small change in the support seems to be responsible for the higher stability of structure A, which is the structure used in subsequent calculations.

Table 6. Change in the Inner Layer of the Support, Calculated with Respect to the 3-Layer-Unreconstructed-TiO_2(001) Slab, upon Deposition of the Vanadia Dimer

structure	Δd^{2nd} (%)	Δd^{3rd} (%)
A	0.26	1.62
B	0.35	1.98
C	0.37	3.16

Appendix D: All Molecularly and Dissociatively Adsorbed Water Configurations Tested

The thermodynamic stability of all hydroxylated and hydrated surfaces tested is shown in Figure 11. The water coverage and the adsorption sites occupied by water for each surface is summarized in Table 1 in the paper. The Gibbs free energy of adsorption was calculated using eq 3 as a function of temperature, yielding a straight line for each surface. The surface associated with the lowest-lying line corresponds to the most stable structure under the given flue gas conditions.

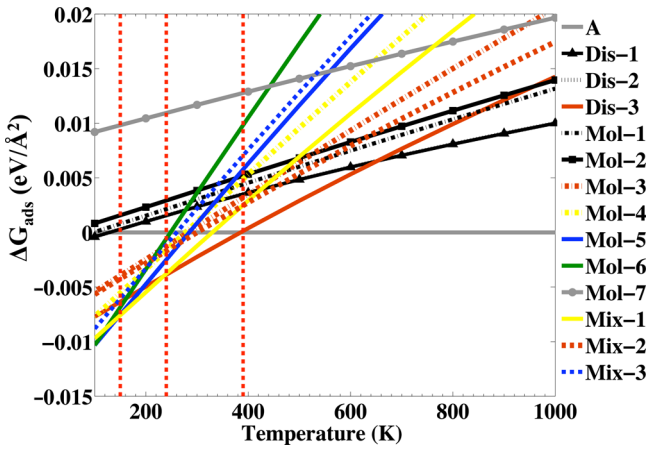

Figure 11. All molecularly and dissociatively adsorbed water configurations tested. The color scheme is the same as in Figure 10 and it is linked to the number of adsorbed water molecules. Green = five water molecules, blue = four water molecules, yellow = three water molecules, red = two water molecules, and black = one water molecule. The gray lines with circles represent the surface where one water molecule is interacting with the vanadia dimer.

At lower temperatures, the lines representing surface with high water coverage (green, blue, and yellow lines that represent 5, 4, and 3 adsorbed water molecules) have more negative Gibbs free energy. However, as the temperature increases, the relative stability is shifted to those surfaces with less adsorbed water (red and black lines that represent 2 and 1 adsorbed water molecules). Surface Mol-7 (grey line with circles) and surface Mol-2 (black line with squares) represent a water molecule interacting with the vanadia dimer and a Ti atom of the support. The relative position of these lines, with Mol-2 lying at lower Gibbs adsorption energy, indicates that water rather interacts with the support than with the vanadia dimer.

Appendix E: PDOS Hydroxylated Surfaces

Figure 12a shows the projected density of states, PDOS, of all oxygen and hydrogen atoms of structures Mol-5 and Dis-3, which represent molecularly and dissociative water adsorption, respectively, for full coverage, that is, $\theta = 1$. Figures 12b and 12c focus on the contribution to the valence band of the individual oxygen and hydrogen atoms involved in the water adsorption modes. Figure 12a shows the relative position of the oxygen and hydrogen peaks for both types of water adsorption, which may be used to compare their relative stabilities. The peaks generated during molecular adsorption of water are located at lower energies, which suggest a higher stability. These results complement the ab initio predictions that indicate higher

dx.doi.org/10.1021/jp310668j | J. Phys. Chem. C 2013, 117, 1761−1772

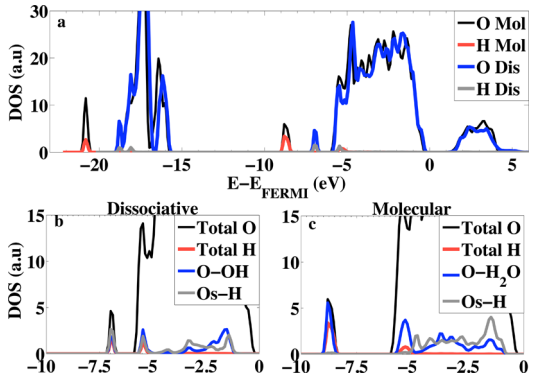

Figure 12. PDOS of the oxygen and hydrogen atoms for both dissociatively and molecularly adsorbed water for full water coverage, that is, $\theta = 1$. Energies are referenced to the calculated Fermi level.

stability for molecular water adsorbed surfaces for the case of high-water coverage. The PDOS of oxygen and hydrogen atoms during water dissociation are represented in Figure 12b, which shows two overlapping O and H peaks at −7 and −5.5 eV, which correspond to the O−H interaction between the two hydroxylated Ti atoms generated during the dissociation of one molecule of water. As described in Figure 2, one of the −OH groups comes from the dissociation of water on a surface Ti atom (labeled as O−OH) and another coming from the breaking of the Ti−O(2) bond during the interaction of the surface O(2) atom coordinate with the −H atom (labeled as Os−H). The lower energy peak, that is, −7 eV, has a larger contribution from the H−Os interaction (grey line), while the −5.5 eV peak has a larger contribution due to the O−H interaction of the hydroxyl group (black line). The PDOS of the oxygen and hydrogen atoms during molecular water adsorption are represented in Figure 12c, which shows a strong peak at −8.7 eV, which is composed mostly by the O−H interaction in the adsorbed water molecule (labeled as O−H_2O). The presence of a second peak at −5.5 eV is due to the H−O interaction between neighboring adsorbed water molecules. The tilted position of the adsorbed water molecule towards the surface also creates a weak interaction between the H atom and a surface oxygen atom, subsequently leading to a small contribution to both peaks (labeled as Os−H).

Appendix F: Dimer Stability as a Function of Water Adsorption: Formation Energies and PDOS

In the Bader charge analysis section, it was suggested that the increase in the charge transfer between the hydroxylated support and vanadia dimer may yield a stronger dimer-support interaction. The relative stability of the vanadia dimer as a function of water adsorption is evaluated by comparing the formation energies of vanadia species on the different hydroxylated/hydrated surfaces. The formation energies, E_{form}, which are summarized in Table 7, were calculated in a similar way as in the TiO_2 slab optimization section, but modifying the formation equation to add the energy of an isolated water molecule as

$$E_{form} = E^{hydr}_{uncon} - [E_{nVO_{2.5}} + E_{TiO_2} + E_{recon} + E^{gas}_{H_2O}] \quad (9)$$

Larger formation energies are obtained with increasing number of adsorbed water, which may be correlated to a higher stability of the vanadia dimer. This stronger bond between the dimer and support may be the result of a larger charge transfer from the adsorbed water to the surface. The increase in the stability of the vanadia dimer is also seen in Figure 13, which presents the change in the PDOS of O(1) and V atoms with the degree of hydroxylation. The contribution to the conduction band of oxygen species is due to the O(2p) density of states. Only the PDOS of the O(1) atom are shown because O(1) is the oxygen atom from the vanadia dimer with the greatest change in charge during the dehydration process.

Table 7. Formation Energies as a Function of Hydroxylation/Hydration

surface	#H_2O	E_{form}
Mol-5	4	−2.48
Mix-1	3	−2.18
Dis-3	2	−1.65
A	0	−0.33

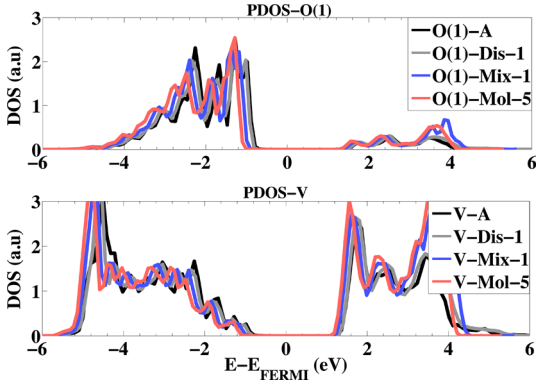

Figure 13. Change in the PDOS of O(1) and V atoms of the vanadia dimer during the dehydration process.

Figure 13 shows a slight shift in both the conduction and valence bands to lower energies with increasing number of adsorbed water molecules. This shift to lower energies supports the idea of increasing stability of the vanadia dimer through charge donation from the adsorbed water to the support.

AUTHOR INFORMATION

Corresponding Author

*E-mail: wilcoxj@stanford.edu.

Notes

The authors declare no competing financial interest.

ACKNOWLEDGMENTS

This work was supported by the Stanford University School of Earth Sciences Graduate Fellowship Program. Computational resources were provided by Stanford's Center for Computational Earth and Environmental Science (CEES). Special recognition is given to Dr. Shela Aboud and Dr. Glenn Jones for their assistance and technical feedback. The authors would also like to thank Abby Kirchofer and Dr. Geoffrey Spikes for their careful review of the manuscript, and to the CEES systems administrator, Dennis Michael.

REFERENCES

(1) United States Environmental Protection Agency, *Mercury and Air Toxics Standards (MATS) for Power Plants*, June 21, 2011.

(2) United States Environmental Protection Agency, *Environmental Footprints and Cost of Coal-Based Integrated Gasification Combined Cycle and Pulverized Coal Technologies*, July, 2006.

(3) Staudt, J. E. *Control technologies to reduce conventional and hazardous air pollutants from coal-fired power plants*; Technical Report, 2011.
(4) Electric Power Research Institute, *EPRI Technical Report No. 1005400*, 2002.
(5) Niksa, S.; Fujiwara, N. *J. Air Waste Manage. Assoc.* **2005**, *55*, 1866−1875.
(6) Brown, T.; Smith, D.; Hargis, R., Jr.; O'Dowd, W. *J. Air Waste Manage. Assoc.* **1999**, *49*, 628−640.
(7) Senior, C.; Linjewile, T. *Oxidation of mercury across SCR catalyst in coal-fired power plants burning low rank fuels*; Technical Report, 2003.
(8) Lietti, L.; Forzatti, P.; Bregani, F. *Ind. Eng. Chem. Res.* **1996**, *35*, 3884−3892.
(9) Alemany, L.; Lietti, L.; Ferlazzo, N.; Forzatti, P.; Busca, G.; Giamello, E.; Bregani, F. *J. Catal.* **1995**, *155*, 117−130.
(10) Lietti, L.; Nova, I.; Forzatti, P. *Top. Catal.* **2000**, *11*, 111−122.
(11) Presto, A.; Granite, E. *Environ. Sci. Technol.* **2006**, *40*, 5601−5609.
(12) Svachula, J.; Alemany, L.; Ferlazzo, N.; Forzatti, P.; Tronconi, E.; Bregani, F. *Ind. Eng. Chem. Res.* **1993**, *32*, 826−834.
(13) Saleh, R.; Wachs, I.; Chan, S.; Chersich, C. *J. Catal.* **1986**, *98*, 102−114.
(14) He, S.; Zhou, J.; Zhu, Y.; Luo, Z.; Ni, M.; Cen, K. *Energy Fuels* **2008**, *23*, 253−259.
(15) Eom, Y.; Jeon, S.; Ngo, T.; Kim, J.; Lee, T. *Catal. Lett.* **2008**, *121*, 219−225.
(16) Vittadini, A.; Casarin, M.; Selloni, A. *Theor. Chim. Acta* **2007**, *117*, 663−671.
(17) Diebold, U. *Surf. Sci. Rep.* **2003**, *48*, 53−229.
(18) Vittadini, A.; Casarin, M.; Sambi, M.; Selloni, A. *J. Phys. Chem. B* **2005**, *109*, 21766−21771.
(19) Vittadini, A.; Casarin, M.; Selloni, A. *J. Phys. Chem. B* **2005**, *109*, 1652−1655.
(20) Vittadini, A.; Selloni, A. *J. Phys. Chem. B* **2004**, *108*, 7337−7343.
(21) Vittadini, A.; Selloni, A.; Rotzinger, F.; Grätzel, M. *Phys. Rev. Lett.* **1998**, *81*, 2954−2957.
(22) Calatayud, M.; Mguig, B.; Minot, C. *Surf. Sci.* **2003**, *526*, 297−308.
(23) Calatayud, M.; Minot, C. *J. Phys. Chem. B* **2004**, *108*, 15679−15685.
(24) Calatayud, M.; Minot, C. *Top. Catal.* **2006**, *41*, 17−26.
(25) Alexopoulos, K.; Hejduk, P.; Witko, M.; Reyniers, M.; Marin, G. *J. Phys. Chem. C* **2010**, *114*, 3115−3130.
(26) Kachurovskaya, N.; Mikheeva, E.; Zhidomirov, G. *J. Mol. Catal. A: Chem.* **2002**, *178*, 191−198.
(27) Herman, G.; Sievers, M.; Gao, Y. *Phys. Rev. Lett.* **2000**, *84*, 3354−3357.
(28) Liang, Y.; Gan, S.; Chambers, S. A.; Altman, E. I. *Phys. Rev. B* **2001**, *63*, 235402.
(29) Silly, F.; Castell, M. *Appl. Phys. Lett.* **2004**, *85*, 3223−3225.
(30) Lazzeri, M.; Vittadini, A.; Selloni, A. *Phys. Rev. B* **2001**, *63*, 155409.
(31) Gong, X.; Selloni, A.; Vittadini, A. *J. Phys. Chem. B* **2006**, *110*, 2804−2811.
(32) Topsoe, N.; Topsoe, H.; Dumesic, J. *J. Catal.* **1995**, *151*, 226−240.
(33) Bond, G. *Appl. Catal. A: Gen.* **1997**, *157*, 91−103.
(34) Wachs, I.; Weckhuysen, B. *Appl. Catal. A: Gen.* **1997**, *157*, 67−90.
(35) Went, G.; Oyama, S.; Bell, A. *J. Phys. Chem.* **1990**, *94*, 4240−4246.
(36) Olthof, B.; Khodakov, A.; Bell, A.; Iglesia, E. *J. Phys. Chem. B* **2000**, *104*, 1516−1528.
(37) Kozlowski, R.; Pettifer, R.; Thomas, J. *The J. Phys. Chem.* **1983**, *87*, 5176−5181.
(38) Haber, J.; Kozlowska, A.; Kozlowski, R. *J. Catal.* **1986**, *102*, 52−63.
(39) Hermann, K.; Witko, M.; Druzinic, R.; Tokarz, R. *Top. Catal.* **2000**, *11*, 67−75.
(40) Sauer, J.; Döbler, J. *Dalton Trans.* **2004**, 3116−3121.
(41) Sun, C.; Dong, L.; Yu, W.; Liu, L.; Li, H.; Gao, F.; Dong, L.; Chen, Y. *J. Mol. Catal. A: Chem.* **2011**, *346*, 29.
(42) Evan, J.; Pennline, H.; Hargis, R. *Ind. Eng. Chem. Res.* **2000**, *39*, 1020−1029.
(43) Presto, A.; Granite, E. *Platinum Metals Rev.* **2008**, *52*, 144−154.
(44) Kresse, G.; Furthmüller, J. *Comput. Mater. Sci.* **1996**, *6*, 15−50.
(45) Perdew, J.; Burke, K.; Ernzerhof, M. *Phys. Rev. Lett.* **1996**, *77*, 3865−3868.
(46) Blochl, P. *Phys. Rev. B* **1994**, *50*, 17953−17979.
(47) Monkhorst, H.; Pack, J. *Phys. Rev. B* **1976**, *13*, 5188−5192.
(48) Wagemaker, M.; Kearley, G.; van Well, A.; Mutka, H.; Mulder, F. *J. Am. Chem. Soc.* **2003**, *125*, 840−848.
(49) Negreira, A. S.; Aboud, S.; Wilcox, J. *Phys. Rev. B* **2011**, *83*, 045423.
(50) Enjalbert, R.; Galy, J. *Acta Crystallogr., Sect. C: Cryst. Struct. Commun.* **1986**, *42*, 1467−1469.
(51) Goclon, J.; Grybos, R.; Witko, M.; Hafner, J. *J. Phys.: Condens. Matter* **2009**, *21*, 095008.
(52) See www.iecm-online.com for technical documentation, current public version of the software, 2007.
(53) United States Environmental Protection Agency, *Evaluation of the Impact of Chlorine on Mercury Oxidation in a Pilot-Scale Coal Combustor; The Effect of Coal Blending*, 2009.
(54) Mason, S.; Iceman, C.; Trainor, T.; Chaka, A. *Phys. Rev. B* **2010**, *81*, 125423.
(55) Reuter, K.; Scheffler, M. *Phys. Rev. B* **2001**, *65*, 035406.
(56) Lo, C.; Tanwar, K.; Chaka, A.; Trainor, T. *Phys. Rev. B* **2007**, *75*, 075425.
(57) Guhl, H.; Miller, W.; Reuter, K. *Phys. Rev. B* **2010**, *81*, 155455.
(58) Aboud, S.; Wilcox, J.; Brown, G. *Phys. Rev. B* **2011**, *83*, 125407.
(59) Rogal, J. *Ab initio atomistic thermodynamics for surfaces: A primer*; Technical Report, 2006.
(60) Blum, R.; Niehus, H.; Hucho, C.; Fortrie, R.; Ganduglia-Pirovano, M.; Sauer, J.; Shaikhutdinov, S.; Freund, H. *Phys. Rev. Lett.* **2007**, *99*, 226103.
(61) Wang, X.; Chaka, A.; Scheffler, M. *Phys. Rev. Lett.* **2000**, *84*, 3650−3653.
(62) Sun, Q.; Reuter, K.; Scheffler, M. *Phys. Rev. B* **2003**, *67*, 205424.
(63) NIST-JANAF. In *NIST-JANAF Thermochemical Tables*, 4th ed.; Chase, J., Ed.; American Chemical Society: Washington, DC, 1998.
(64) Lazzeri, M.; Selloni, A. *Phys. Rev. Lett.* **2001**, *87*, 266105.
(65) Blomquist, J.; Walle, L.; Uvdal, P.; Borg, A.; Sandell, A. *J. Phys. Chem. C* **2008**, *112*, 16616−16621.
(66) Padak, B.; Brunetti, M.; Lewis, A.; Wilcox, J. *Environ. Progr.* **2006**, *25*, 319−326.
(67) Padak, B.; Wilcox, J. *Carbon* **2009**, *47*, 2855−2864.
(68) Sliger, R.; Kramlich, J.; Marinov, N. *Fuel Process. Technol.* **2000**, *65*, 423−438.
(69) Horne, D.; Gosavi, R.; Strausz, O. *J. Chem. Phys.* **1968**, *48*, 4758.
(70) Wilcox, J. *J. Phys. Chem. A* **2009**, *113*, 6633−6639.
(71) Jones, G.; Jakobsen, J.; Shim, S.; Kleis, J.; Andersson, M.; Rossmeisl, J.; Abild-Pedersen, F.; Bligaard, T.; Helveg, S.; Hinnemann, B.; Jones, G.; Jakobsen, J. G.; Shim, S. S.; Kleis, J.; Andersson, M. P.; Rossmeisl, J.; Abild-Pedersen, F.; Bligaard, T.; Helveg, S.; Hinnemann, B.; et al. *J. Catal.* **2008**, *259*, 147−160.
(72) Calatayud, M.; Minot, C. *Surf. Sci.* **2004**, *552*, 169−179.
(73) Wang, J.; Fan, C.; Sun, Q.; Reuter, K.; Jacobi, K.; Scheffler, M.; Ertl, G. *Angew. Chem., Int. Ed.* **2003**, *42*, 2151−2154.